Citation
Wang, K. and El-Mowafy, A. and Yang, X. 2023. Integer ambiguity Resolution in Multi-constellation GNSS for LEO Satellites POD. In: Institute of Navigation (ION) GNSS+ 2023, 11-15 September 2023, Denver, Colorado.

Integer Ambiguity Resolution in Multi-Constellation GNSS for LEO satellite POD

Kan Wang, *National Time Service Center, Chinese Academy of Sciences, Xi'an, China; University of Chinese Academy of Sciences, Beijing, China*
Ahmed El-Mowafy, *School of Earth and Planetary Sciences, Curtin University, Perth, Australia*
Xuhai Yang, *National Time Service Center, Chinese Academy of Sciences, Xi'an, China; University of Chinese Academy of Sciences, Beijing, China*

Biographies

Kan Wang is a Professor at the National Time Service Center, Chinese Academy of Sciences. She received her PhD in GNSS advanced modeling from ETH Zurich in 2016. Her research interests include high-precision GNSS positioning, LEO-augmented PNT service, LEO satellite POD and clock determination, and integrity monitoring.
Ahmed El-Mowafy is a Professor of Positioning and Navigation, leader of the GNSS research group, and Director of Graduate Research, School of Earth and Planetary Sciences, Curtin University, Australia. He obtained his Ph.D. from the University of Calgary, Canada, in 1995. He has more than 220 publications in precise positioning and navigation using GNSS, quality control, integrity monitoring and estimation theory.
Xuhai Yang is a Professor at the National Time Service Center, Chinese Academy of Sciences. Since 2007, he has served as the director of the research department of high-precision time transfer and precise orbit determination. His research interests include high-precision time transfer, orbit measurement, orbit determination.

Abstract

Precise Orbit Determination (POD) of Low Earth Orbit (LEO) satellites is essential for future LEO-augmented Positioning, Navigation and Timing (PNT) service based on the use of Global Navigation Satellite Systems (GNSS) measurements. Compared with the ambiguity-float LEO satellite POD, Integer Ambiguity Resolution (IAR) reduces number of parameters, eliminates the high correlations between the ambiguities and other estimable parameters, and strengthens model strength. In this study, using real data from Sentinel-6A tracking dual-frequency GPS and Galileo observations, the wide-lane (WL) and narrow-lane (NL) ambiguity fixing rates and the effects of the IAR on orbital accuracy are assessed in the single- and dual-constellation scenarios. Post-processed high-accuracy GNSS satellite clocks, orbits and Observable-specific Signal Biases (OSBs) from the final products of the Center for Orbit Determination in Europe (CODE) and the rapid products of the GeoForschungsZentrum (GFZ) are used for the analysis. Results showed that both the WL and NL fixing rates in the Galileo-only scenario are higher than those in the GPS-only scenario, reaching more than 98%. This implies a better signal quality of the Galileo observations. Applying IAR has improved the orbital accuracy for all single- and dual-constellation scenarios, and was shown to be especially helpful in reducing the once-per-revolution systematic effects in the along-track orbital errors, with over 50% improvement when using the COM products. With the IAR enabled, when using the COM final products, the 3D RMS of the orbital errors amounts to 1.2, 1.2 and 1.1 cm in the GPS-only, Galileo-only and GPS+Galileo combined scenarios, and the RMS of the Orbital User Range Errors (OUREs) amounts to 0.7, 0.7 and 0.6 cm, respectively. When using the GFZ rapid products, the IAR-enabled 3D RMS were 1.8, 2.1 and 1.4 cm in the GPS-only, Galileo-only and GPS+Galileo combined scenarios, with OURE RMS of about 1 cm.

1. INTRODUCTION

Precise Orbit Determination (POD) of Low Earth Orbit (LEO) satellites has gained increased attention in recent years due to the growing need for it in different applications. Among them, the LEO-augmented GNSS (Global Navigation Satellite System) precise positioning, which sets high accuracy requirements for the LEO satellite orbits and clocks at the cm-level similar to the high-precision GNSS products. The augmentation of LEO satellites brings numerous advantages to traditional GNSS-based Positioning, Navigation,

and Timing (PNT) services (Reid et al., 2018). The much lower orbital altitudes of LEO satellites ranging from a few hundred kilometers to 1500 km (Montenbruck & Gill, 2000) guarantee a faster speed, stronger signal strength, and lower cost. Firstly, The fast speed of LEO satellites, around 7-8 km/s, accelerates the satellite geometry change in view of a ground-based user, which is beneficial for shortening the convergence time of the Precise Point Positioning (PPP) (Ge et al., 2018; Li et al., 2018a) and the wide-area PPP – Real-Time Kinematic (PPP-RTK) positioning (Wang et al., 2022). The faster speed is also helpful to whiten multipath effects (Faragher & Ziebart, 2020), which is a bottleneck of GNSS positioning in urban areas. Secondly, benefiting from the much lower orbital heights of the LEO satellites compared to the GNSS satellites at the Medium Earth Orbit (MEOs) or Geosynchronous Orbits (GEOs), the signals transmitted by LEO satellites are around 30 dB stronger than those of GNSS satellites (GPS World Staff, 2017), which is advantageous for, e.g., anti-jamming. Thirdly, the lower cost allows for the launch of a large number of LEO satellites, as seen for diverse LEO constellations launched for various purposes including communication and navigation (Yang, 2019; Michalak et al., 2021; Reid et al., 2022; Wang et al., 2022). Among them, those are ready to transmit navigation signals should significantly be able to improve the satellite geometry, especially in challenging GNSS environments with limited satellite numbers visible to users (Lawrence et al., 2017).

To make use of these benefits, high-precision orbits and clocks of LEO satellites are needed. Nowadays, LEO satellite orbits can be determined with high accuracy by combining GNSS observations collected onboard and dynamic models in a reduced-dynamic processing approach. For the post-processing mode, the ambiguity-float POD can reach the cm-level using dual-frequency GNSS phase and code observations and final GNSS clocks and orbits from different analysis centers (Li et al., 2018; Wang et al., 2020). With the integer ambiguities resolved, the post-processed POD can reach 1 cm accuracy, as reported by Mao et al., (2020) using dual-frequency GPS observations, and Montenbruck et al., (2021) using dual-frequency GPS+Galileo combined observations. For the real-time or near-real-time POD, the orbital accuracy is often limited by the accuracy of the real-time GNSS products used. Based on a batch least-squares adjustment with high-precision real-time GNSS products, the POD accuracy can reach a few centimeters to about 1 dm depending on the real-time GNSS products used (Allahvirdi-Zadeh et al., 2021). Using Kalman filtering, the real-time POD accuracy can also generally reach sub-dm to dm-level using dual-frequency GPS observations (Montenbruck et al., 2013; Hauschild et al., 2016) or GPS+Galileo combined observations (Hauschild et al., 2022).

Correct Integer Ambiguity Resolution (IAR) has numerous advantages in the LEO satellite POD. For example, it reduces the number of estimable parameters and enables a stronger observation mode, it removes the correlations between ambiguities and other parameters, such as the LEO satellite clock offsets, and thus enables improved precision for these parameters. However, compared to the ambiguity-float POD, which also exhibits good accuracy in the post-processing mode, applying IAR requires additional information , i.e. the Observable-specific Signal Biases (OSBs) to separate the ambiguities from the GNSS satellite phase biases (Duan and Hugentobler 2021; Su et al., 2022; Geng et al., 2022). One should also consider that wrong ambiguity resolution would affect the POD accuracy. Moreover, after fixing the ambiguities, errors in the considered hardware biases, the GNSS satellite clocks and orbits, or other mis-modeled biases, do not have the chance to be absorbed by the float ambiguity parameters.

With the public observation and attitude data of Sentinel-6A tracking dual-frequency measurements on both the GPS L1/L2 and Galileo E1/E5a signals, collected onboard LEO satellites, it is possible to assess the IAR success rates and the achieved POD accuracy in single-constellation scenarios of GPS and Galileo, and the GPS + Galileo combined mode. In this study, based on the batch least-squares adjustment in the post-processed mode, the fixing rates of the wide-lane (WL) and narrow-lane (NL) ambiguities of Sentinel-6A are evaluated together with its orbital accuracy in the radial, along-track, cross-track, and Earth-oriented directions, with the last term expressed in the form of the Orbital User Range Error (OURE). High-accuracy multi-GNSS orbits, clocks, and hardware biases from different analysis centers are used for the IAR and POD, including those from the Center for Orbit Determination in Europe (CODE) (Villiger et al., 2019; Schaer et al., 2021) and the GeoForschungsZentrum (GFZ) (Männel et al., 2020).

The paper starts with a short introduction of the applied strategies for ambiguity resolution and the LEO satellite POD. It is followed by the test results including the fixing rates of the WL and the NL ambiguities for the GPS-only, Galileo-only, and GPS + Galileo combined scenarios using GNSS products from different institutions (Code and GFZ). POD accuracy that can be achieved for the ambiguity-float and IAR-enabled cases under different scenarios is then assessed. The conclusions are given at the end.

2. PROCESSING STRATEGY

Before processing, the multi-GNSS phase and code observations need to be scanned for cycle slip detection and repair and outlier exclusion, etc. (Dach et al., 2015; Wang & El-Mowafy, 2020). Afterwards, the processing can generally be split into two parts, i) ambiguity resolution; and ii) the batch least-squares POD. In this section, the procedures of these two parts are described in detail.

2.1. Ambiguity Resolution

With the help of the post-processed GNSS satellite orbits, clocks and OSBs, the ambiguity resolution is performed in two steps, i.e., first resolving the WL ambiguities, defined as $N_{r,\mathrm{WL}}^{s}$ using the Melbourne-Wübbena (MW) combination, and then resolving the NL ambiguities, denoted as $N_{r,\mathrm{NL}}^{s}$ using the ionosphere-free (IF) combination with the WL ambiguities introduced in their solution.

The MW combination is known as a geometry-free (GF) and IF combination, which removes the first-order ionospheric delays and geometry-related errors such as the satellite and receiver clocks. According to the observation equation (1), the remaining terms in the MW combination ($p_{r,\mathrm{MW}}^{s}$) are only the WL ambiguities and the MW receiver bias ($b_{r,\mathrm{MW}}$) and satellite biases (b_{MW}^{s}), expressed as:

$$\begin{aligned}\mathrm{E}\left(p_{r,\mathrm{MW}}^{s}\right) &= \frac{f_1\varphi_{r,1}^{s} - f_2\varphi_{r,2}^{s}}{f_1 - f_2} - \frac{f_1 p_{r,1}^{s} + f_2 p_{r,2}^{s}}{f_1 + f_2} \\ &= \underbrace{\frac{c}{f_1 - f_2}}_{\lambda_{\mathrm{WL}}} N_{r,\mathrm{WL}}^{s} + \underbrace{\left(\frac{f_1\delta_{r,1} - f_2\delta_{r,2}}{f_1 - f_2} - \frac{f_1 d_{r,1} + f_2 d_{r,2}}{f_1 + f_2}\right)}_{b_{r,\mathrm{MW}}} - \underbrace{\left(\frac{f_1\delta_1^{s} - f_2\delta_2^{s}}{f_1 - f_2} - \frac{f_1 d_1^{s} + f_2 d_2^{s}}{f_1 + f_2}\right)}_{b_{\mathrm{MW}}^{s}}\end{aligned} \tag{1}$$

where $\varphi_{r,j}^{s}$ and $p_{r,j}^{s}$ denote the phase and code observations from GNSS satellite s collected onboard LEO satellite r on the j-th frequency of the corresponding constellation, respectively, and f_1 and f_2 are the first and the second frequency used for the corresponding constellation. c denotes the speed of light. $\delta_{r,j}$ and $d_{r,j}$ represent the receiver phase and code biases on the j-th frequency, respectively, and δ_j^{s} and d_j^{s} are their counterparts for GNSS satellites. E(·) is the expectation operator to ignore the noise, assumed to be Gaussian with zero mean, in the equations. The WL wavelength λ_{WL} is about 86 cm for GPS L1 (1575.42 MHz) and L2 (1227.6 MHz), and about 75 cm for Galileo E1 (1575.42 MHz) and E5a (1176.45 MHz).

With the OSBs of the GNSS satellites introduced into Eq. (1), the b_{MW}^{s} are corrected. The WL ambiguities N_{WL} are then solved together with the MW code biases of the LEO satellite, with the latter term assumed to be constant over the processing period. To avoid singularities between the WL ambiguities $N_{r,\mathrm{WL}}^{s}$ and the MW receiver biases $b_{r,\mathrm{MW}}$,the $b_{r,\mathrm{MW}}$ are constrained to zeros in the first least-squares adjustment. The observation equation can then be re-formulated as follows:

$$\mathrm{E}\left(p_{r,\mathrm{MW}}^{s} + b_{\mathrm{MW}}^{s}\right) = \lambda_{\mathrm{WL}} N_{r,\mathrm{WL}}^{s} + b_{r,\mathrm{MW}} \tag{2}$$

The estimated WL ambiguities ($\hat{N}_{r,\mathrm{WL}}^{s}$) are formed to single-differenced ambiguities on the between-satellite level or between-track level (for the same satellite, if considered) ($\hat{N}_{r,\mathrm{WL}}^{us}$) and solved to integers ($\tilde{N}_{r,\mathrm{WL}}^{us}$). Various methods can be used for the IAR based on the float values of the estimated ambiguities and their variance-covariance matrices. In this study, the SIGMA-dependent method (Dach et al., 2015) is used to resolve the ambiguities iteratively in an ascending order of their a posteriori formal standard deviations. The fixed between-satellite ambiguities are introduced into the observation equations for resolving the next ones. The ambiguity is only resolved when there is one integer value lays within $\pm\beta\sigma_{ij}$, where σ_{ij} denotes the a posteriori formal standard deviations of the between-satellite ambiguity to be resolved. σ_{ij} is not allowed to exceed a pre-defined threshold of α cycles for the resolved ambiguities. As the WL wavelength is large, with good quality GNSS products, the WL ambiguities can normally be resolved with a large fixing rate.

In the next step, the resolved WL ambiguities are introduced into the IF combination of the phase observations ($\varphi_{r,\mathrm{IF}}^{s}$), which can be expressed as:

$$\mathrm{E}\left(\Delta\varphi_{r,\mathrm{IF}}^{s}\right)=\frac{f_1^2\varphi_{r,1}^{s}-f_2^2\varphi_{r,2}^{s}}{f_1^2-f_2^2}$$

$$=A_{\mathrm{orb}}X_{\mathrm{orb}}+c\times\Delta t_r+\frac{f_2}{f_1-f_2}\lambda_{\mathrm{WL}}N_{r,\mathrm{WL}}^{s}+\underbrace{\frac{c}{f_1+f_2}}_{\lambda_{\mathrm{NL}}}N_{r,1}^{s}+\underbrace{\frac{f_1^2\delta_{r,1}-f_2^2\delta_{r,2}}{f_1^2-f_2^2}}_{b_{r,\mathrm{IF}}}-\underbrace{\frac{f_1^2\delta_1^{s}-f_2^2\delta_2^{s}}{f_1^2-f_2^2}}_{b_{\mathrm{IF}}^{s}} \tag{3}$$

where $\Delta\varphi_{r,\mathrm{IF}}^{s}$ is the IF Observed-Minus-Computed (O-C) term, having the phase windup, LEO and GNSS satellite antenna sensor offsets, Phase Center Offsets (PCOs) and Variations (PCVs) corrected. X_{orb} are the estimable orbital dynamic parameters, which include the six Keplerian elements, three constant terms for the Solar Radiation Pressure (SRP) parameters in the radial, along-track and cross-track directions, and stochastic velocity pulses in these three directions separated by 15 min each. The stochastic velocity pulses are constrained to zeros with a standard deviation of 5×10^{-6} m/s. A_{orb} corresponds to the partial derivatives of the IF phase observations with respect to X_{orb}, which is numerically integrated into each processing epoch based on the variational equations (Montenbruck & Gill, 2000). Δt_r denotes the LEO satellite clock bias. $N_{r,1}^{s}$ is the ambiguity for LEO satellite r, GNSS satellite s on the first frequency of the corresponding constellation. The NL wavelength λ_{NL} is about 10.7 cm for GPS L1 and L2, and about 10.9 cm for Galileo E1 and E5a.

With the GNSS OSBs and the resolved single-differenced WL ambiguities $\breve{N}_{r,\mathrm{WL}}^{us}$ introduced, Eq. (3) can be re-formulated as:

$$\mathrm{E}\left(\varphi_{r,\mathrm{IF}}^{s}+b_{\mathrm{IF}}^{s}-\frac{f_2}{f_1-f_2}\lambda_{\mathrm{WL}}\breve{N}_{r,\mathrm{WL}}^{us}\right)=A_{\mathrm{orb}}X_{\mathrm{orb}}+c\times\Delta\tilde{t}_r+\lambda_{\mathrm{NL}}N_{r,1}^{1s} \tag{4}$$

with the LEO satellite IF phase biases $b_{r,\mathrm{IF}}$ and the reference ambiguity $N_{r,1}^{1}$ absorbed by the LEO satellite clock parameter, such that:

$$\Delta\tilde{t}_r=\Delta t_r+\frac{b_{r,\mathrm{IF}}}{c}+\frac{f_2}{c(f_1-f_2)}\lambda_{\mathrm{WL}}N_{r,\mathrm{WL}}^{u}+\frac{\lambda_{\mathrm{NL}}}{c}N_{r,1}^{1} \tag{5}$$

In such a case, the orbital dynamic parameters X_{orb}, the epoch-wise LEO satellite clock $\Delta\tilde{t}_r$ and the ambiguities $N_{r,1}^{1s}$ remain to be solved in a least-squares adjustment. The estimated float ambiguities $\widehat{N}_{r,1}^{1s}$ are then formed into new single-differenced NL ambiguities $\widehat{N}_{r,1}^{vs}$ on the between-satellite or between-track level (for the same satellite) for a better resolution. The float single-differenced ambiguities are solved to integers ($\breve{N}_{r,1}^{vs}$) with the SIGMA-dependent method.

2.2. LEO satellite POD

The resolved WL and NL ambiguities ($N_{r,\mathrm{WL}}^{us}$ and $N_{r,1}^{vs}$) are all introduced into Eq. (3), andthe phase O-C term can then be re-formulated as:

$$\mathrm{E}\left(\varphi_{r,\mathrm{IF}}^{s}+b_{\mathrm{IF}}^{s}-\frac{f_2}{f_1-f_2}\lambda_{\mathrm{WL}}\breve{N}_{r,\mathrm{WL}}^{us}-\lambda_{\mathrm{NL}}\breve{N}_{r,1}^{vs}\right)=\tilde{A}_{\mathrm{orb}}\tilde{X}_{\mathrm{orb}}+c\times\Delta\tilde{\tilde{t}}_r \tag{6}$$

with

$$\Delta\tilde{\tilde{t}}_r=\Delta t_r+\frac{b_{r,\mathrm{IF}}}{c}+\frac{f_2}{c(f_1-f_2)}\lambda_{\mathrm{WL}}N_{r,\mathrm{WL}}^{u}+\frac{\lambda_{\mathrm{NL}}}{c}N_{r,1}^{v} \tag{7}$$

Note that in this final POD procedure, the estimable orbital parameters $\tilde{X}_{\mathrm{orb}}$ differ from those in Eq. (4), i.e., X_{orb}. The $\tilde{X}_{\mathrm{orb}}$ include six Keplerian elements, three constant terms of the SRP parameters, and piece-wise constant accelerations separated by 6 min in the radial, along-track and cross-track directions. The piece-wise constant accelerations are constrained to zeros with a standard deviation of 5×10^{-9} m/s^2. $\tilde{A}_{\mathrm{orb}}$ corresponds to the partial derivatives of the IF phase observations with respect to the orbital parameters

$\tilde{X}_{\mathrm{orb}}$. The orbital parameters $\tilde{X}_{\mathrm{orb}}$ and the estimable LEO satellite clocks $\Delta\tilde{\tilde{t}}_r$ are estimated in a least-squares adjustment using only the phase measurements.

With the orbital dynamic parameters estimated, the 3D Cartesian orbits can be numerically integrated into each processing epoch based on existing dynamic models and the estimated model improvements. In this study, the EGM2008 (Pavlis et al., 2008) is applied to the Earth's gravitational attraction, with an Earth potential degree of 120. The gravitational attraction is also considered for other planets using the JPL DE421 ephemeris (Folkner et al., 2009). The solid Earth tides and pole tides are modeled based on the IERS 2010 (Petit & Luzum, 2010), and the ocean tides are based on the FES2014b model (Lyard et al., 2006).

2.3. Calibration

The pre-condition for high-precision POD of the Center of Mass (CoM) of the LEO satellite is the highly accurate knowledge of the PCO/PCV information and the onboard Antenna Sensor Offset (ASO) information. As the CoM drifts with time, and its knowledge of the test satellite in this study, i.e., the Sentinel-6A, is not yet fully open to the public, the 3-dimensional (3D) vector from the CoM of the GPS IF Antenna Phase Center (APC) is directly determined in the satellite body-fixed frame in this contribution, based on the IAR-enabled GPS+Galileo combined APC solutions and the reference orbits provided by the Copernicus POD service (CSPDH, 2023). The difference between the Galileo IF PCO and the GPS IIF PCO is about 18 mm in the up direction of the antenna (Montenbruck et al., 2021), and is considered in the calculation.

The vector from the CoM to the GPS IF APC, denoted as ΔX_{BFS}, is determined in the satellite body-fixed frame as:

$$\Delta X_{\mathrm{BFS}} = R_{\mathrm{I2B}} \Delta X_{\mathrm{ECI}} \tag{8}$$

where ΔX_{ECI} is the mean difference between the calculated IAR-enabled GPS + Galileo combined APC orbits and the CoM reference orbits in the inertial frame. R_{I2B} is the rotation matrix from the inertial frame to the body-fixed frame, calculated based on the attitude information tracked onboard the LEO satellite.

3. TEST RESULTS

In this study, the dual-frequency phase and code observations on the GPS L1 (C or W signals) / L2 (L or W signals) and Galileo E1C and E5aQ from February 1 to 7, 2022, are used for the IAR and POD processes. The processing is performed on a daily basis with a sampling interval of 30 s. Equal weight is applied when considering elevation-angle dependency in both the IAR and POD. The a priori standard deviations for phase and code observations are set to 0.001 and 0.1 m, respectively. The GPS and Galileo clocks, orbits and OSBs are taken from two different institutions, assumed to be compatible, with details given in Table 1. In this section, the fixing rates and the resulting IAR-enabled POD results will be discussed in the following two sub-sections.

Table 1

Details of the multi-GNSS products from CODE and GFZ within the test week

Institution	Index	Product Type	Latency	Products			
				Clocks	Orbits	OSBs	
						GPS (L1 & L2)	Galileo (E1 & E5a)
CODE	COM	Final	~ 12 days	30 s	5 min	C1C/C1W/C2C/C2W L1C/L1W/L2C/L2W/L2X	C1C/C1X/C5Q/C5X L1C/L1X/L5Q/L5X
GFZ	GBM	Rapid	24 h (Deng et al., 2017)	30 s	5 min	C1W/C2W L1W/L2W	C1C/C5Q L1C/L5Q

3.1. Fixing rate

The ambiguity fixing rates are, on one side, related to the observation quality and the accuracy of the introduced GNSS products, and on the other side, related to the criterion for resolving them. For the SIGMA-dependent method, as discussed before, the a posteriori standard deviation should not exceed a pre-defined threshold of α cycles, and only one integer should lie in the confidence

interval of $\pm\beta\sigma_{ij}$. Strict α and β are helpful to guarantee correct ambiguity resolution. However, they may also make some resolvable ambiguities remain unresolved.

Setting a strict α of 0.05 cycles, and β of 6, the fixing rates of the WL ambiguities are listed in Table 2 when using different GNSS products (see Table 1). It can be observed from the table that for both GNSS products used in the tests, the fixing rates in the Galileo-only scenario are higher than both the GPS-only and the GPS + Galileo combined scenarios. This suggests better Galileo code observation quality, which is essential in the MW combination and for the WL ambiguity resolution. The averaged GPS-only WL fixing rates are slightly below 90% using both products, whereas the Galileo-only WL fixing rates are all above 95%. The WL fixing rate using the two GNSS products are similar to each other.

Table 2

Fixing rates(in percentage) of the WL ambiguities using GNSS products from different institutions. "G", "E" and "G + E" represent the GPS-only, Galileo-only and GPS+Galileo combined scenarios

DOY in 2022	COM (%)			GBM (%)		
	G	E	G + E	G	E	G + E
032	89.84	99.63	95.23	89.84	99.63	95.23
033	88.42	91.88	90.55	90.03	99.63	95.02
034	82.17	98.87	90.34	81.85	99.25	90.52
035	90.06	99.60	94.32	90.06	99.60	94.32
036	90.00	99.62	94.69	90.31	100.00	94.86
037	89.27	100.00	94.13	88.96	100.00	94.30
038	89.10	100.00	94.43	88.78	100.00	94.25
Average	88.41	98.52	93.38	88.55	99.73	94.07

The NL ambiguity fixing is more challenging than that of the WL. Table 3 lists the fixing rates of the NL ambiguity resolution using the same criterion of the SIGMA-dependent strategy. It should be noted that the NL ambiguity resolution is not performed on certain days due to the strict criterion set in the SIGMA-dependent strategy. Still, using the GBM products, one can obtain an NL fixing rate of about 94% in the GPS+Galileo combined case.

Table 3

Fixing rates (in percentage) of the NL ambiguities using GNSS products from different institutions with α set to 0.05 cycles. "G", "E" and "G + E" represent the GPS-only, Galileo-only and GPS+Galileo combined scenarios.

DOY in 2022	COM (%)			GBM (%)		
	G	E	G + E	G	E	G + E
032	88.85	99.63	95.05	88.85	99.26	94.88
033	0	0	0	89.71	99.26	95.02
034	57.37	99.25	90.64	55.45	98.49	90.47
035	90.32	99.60	94.47	8.71	99.20	94.30
036	89.94	99.62	94.67	89.31	99.24	94.33
037	89.52	100.00	94.11	87.94	99.62	93.76
038	89.03	100.00	94.23	68.39	99.62	94.23
Average	72.15	85.44	80.45	69.76	99.24	93.85

When setting the maximum tolerable value of the aposteriori standard deviation of the ambiguities (α) to 0.07 cycles, the NL fixing rates on the Day of Year (DOY) 033 and 034 have increased when using the COM products, as shown in Table 4. The same also occurred for DOY 034, 035 and 038 when using the GBM products. On DOY 033, the 3D RMSE of the COM-based orbits have decreased from 1.6, 2.0, and 1.7 cm using α of 0.05 cycles in the GPS-only, Galileo-only and GPS+Galileo combined cases, respectively, to 1.2, 1.2 and 1.1 cm when increasing α to 0.07 cycles. This suggests that the parameter α could be a limiting factor for the NL ambiguity resolution in the SIGMA-dependent method, and a proper α value should be tested for relevant GNSS products

to balance between the fixing rate and the correctness of the NL ambiguity resolution. Accordingly, in the following contexts, α is set to 0.07 cycles for the NL ambiguity resolution.

Table 4

Fixing rates (in percentage)of the NL ambiguities using GNSS products from different institutions with α set to 0.07 cycles. "G", "E" and "G + E" represent the GPS-only, Galileo-only and GPS+Galileo combined scenarios

DOY in 2022	COM (%)			GBM (%)		
	G	E	G + E	G	E	G + E
032	88.85	99.63	95.05	88.85	99.26	94.88
033	88.42	91.88	90.55	89.71	99.26	95.02
034	82.37	99.25	90.64	80.77	98.49	90.47
035	90.32	99.60	94.47	87.74	99.20	94.47
036	89.94	99.62	94.67	89.31	99.62	94.33
037	89.52	100.00	94.11	87.94	99.62	93.76
038	89.03	100.00	94.23	87.74	99.62	94.23
Average	88.35	98.57	93.39	87.44	99.30	93.88

3.2. Orbital accuracy

To assess the orbital accuracy, the reference orbits provided by the Copernicus POD service (CSPDH, 2023) that exhibit a 3D RMSE accuracy of about 1 cm (Montenbruck et al., 2021) are used for comparison. Although the ambiguity-float POD solutions already reach a high accuracy using post-processing GNSS products using a least-squares adjustment, fixing ambiguities is helpful to further improve the accuracy to 1 cm or better. Figure 1 shows the radial (ΔR), along-track (ΔS) and cross-track (ΔW) orbital errors in the ambiguity-float and IAR-enabled cases under the GPS+Galileo combined scenario using Sentinel-6A data on February 4, 2022. It can be seen that compared to the red lines of the ambiguity-float case, the IAR helps to reduce the once-per-revolution systematic effects and stabilizes the results, especially in the along-track direction. In the IAR-enabled case (blue lines), on this test day, the RMS of the radial, along-track and cross-track orbital errors amount to about 5 mm, 5 mm and 6 mm, respectively. The 3D RMSE is about 9 mm. The σ_{OURE} amounts to about 5 mm and is calculated as the RMS of the orbital errors projected onto the Earth's direction in a global averaged sense. It can be expressed as:

$$\sigma_{\mathrm{OURE}} = \sqrt{\omega_{\mathrm{R}}^2 \sigma_{\mathrm{R}}^2 + \omega_{\mathrm{SW}}^2 (\sigma_{\mathrm{S}}^2 + \sigma_{\mathrm{W}}^2)} \tag{9}$$

where σ_{R}, σ_{S} and σ_{W} represent the RMS of the orbital errors in the radial, along-track and cross-track directions, respectively. The projection coefficients ω_{R} and ω_{SW} are calculated with the orbital altitude (Chen et al., 2013). For Sentinel-6A of about 1346 km during the test week, ω_{R} is about 0.64 and ω_{SW} is about 0.54.

Figure 1

Orbital errors of Sentinel-6A on February 4, 2022, in the GPS+Galileo combined scenario using COM products in the ambiguity-float and IAR-enabled cases

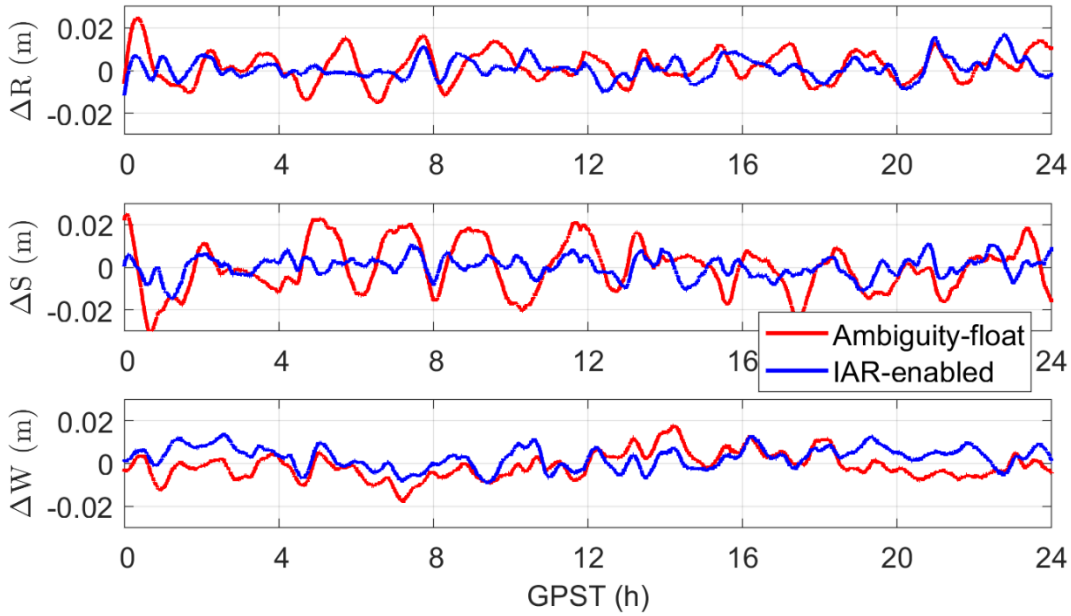

The improved orbital accuracy is not a coincidence. Figure 2 shows the averaged 3D RMSE over the test week in the ambiguity-float and the IAR-enabled cases. The COM and GBM products were used for processing. It can be observed that the improvements brought by the IAR exist in all single- and dual-constellation scenarios and using both the tested GNSS products. The IAR-enabled orbital errors generally have a 3D RMSE of about 1-2 cm. For the GPS+Galileo combined case, it is lower than 1.5 cm. Considering that the reference orbits are not error-free, the 3D RMSE of the true orbital errors calculated in the IAR-enabled mode should even be smaller. The orbital accuracy using the COM final products is slightly better than those using the GBM rapid products.

Figure 2

Averaged 3D RMSE of the ambiguity-float and IAR-enabled orbital errors using (left) the COM products, and (right) the GBM products

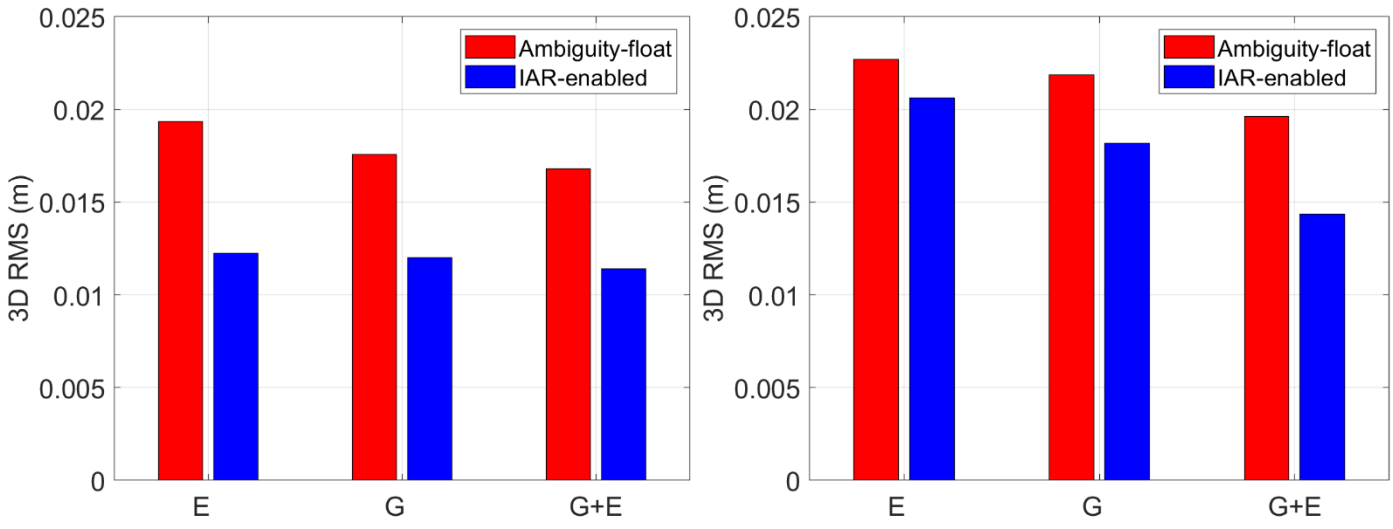

Table 5 lists the averaged RMS of the orbital errors in different directions. It can be seen that the IAR has improved the ambiguity-float orbital errors. The improvements are especially significant in the along-track direction, amounting to more than 50%

when using the COM products in the GPS+Galileo combined case. The improvements are generally bigger when using the COM final products, which exhibit better orbital accuracy in both the ambiguity-float and IAR-enabled solutions. The IAR-enabled GPS+Galileo combined solutions exhibit the best orbital accuracy, i.e., about 1 to 1.5 cm. The differences in the RMSE between single- and dual-constellation orbits are within a few millimeters.

Table 5

Averaged RMS of different types of orbital errors for the ambiguity-float and IAR-enabled cases, and the improvements brought by the ambiguity resolution.

Type	COM			GBM		
	G	E	G + E	G	E	G + E
Ambiguity-float orbital errors (cm)						
Radial	0.8	1.0	0.8	0.9	1.1	0.9
Along-track	1.2	1.4	1.1	1.4	1.5	1.2
Cross-track	1.0	1.0	1.0	1.4	1.3	1.2
3D RMSE	1.8	1.9	1.7	2.2	2.3	2.0
OURE	1.0	1.1	1.0	1.2	1.3	1.1
IAR-enabled orbital errors (cm)						
Radial	0.6	0.6	0.5	0.9	1.1	0.7
Along-track	0.6	0.6	0.5	1.0	1.3	0.7
Cross-track	0.9	0.9	0.9	1.3	1.2	1.0
3D RMSE	1.2	1.2	1.1	1.8	2.1	1.4
OURE	0.7	0.7	0.6	1.0	1.2	0.8
Improvements (%)						
Radial	30.47	39.94	32.72	72	-3.3	17.4
Along-track	52.41	55.85	51.93	30.7	17.8	47.3
Cross-track	11.98	7.42	13.70	8.6	6.3	14.8
3D RMSE	31.73	36.76	32.13	16.9	9.1	26.8
OURE	31.64	37.03	32.18	16.2	8.0	26.1

4. CONCLUSIONS

The high-accuracy LEO satellites orbital products are essential for realizing the high-precision LEO/GNSS-integrated PNT services in the near future. Nowadays, the ambiguity-float LEO satellite POD can achieve high accuracy by combining the dynamic models with the GNSS observations tracked onboard in the so-called reduced-dynamic mode, i.e., at centimeters in the post-processing mode and at the sub-dm level in the real-time mode. With the OSBs introduced in the processing in addition to the high-precision GNSS orbits and clocks, IAR can be enabled by resolving the WL ambiguities first, and then the NL ambiguities. The IAR helps with the de-correlation of the ambiguity parameters with other parameters, such as the LEO satellite clocks, not to mention the significant reduction of the number of estimable parameters. Benefiting from these factors, the observation model is greatly improved after resolving the ambiguities. However, the IAR may also enlarge the projection of the mis-modeled errors into the other parameters. Wrong ambiguity resolution also leads to extra biases in the orbital solutions.

Compared with the traditional GPS-only scenario, the LEO satellite POD has nowadays the chance to benefit from multi-constellation observations. Using the dual-frequency GPS (L1/L2) and Galileo (E1/E5a) observations from Sentinel-6A as an example, the effects of the IAR on the reduced-dynamic orbital errors are assessed in the GPS-only, Galileo-only and GPS+Galileo combined scenarios using the COM final GNSS products and the rapid products from the GFZ. In general, proper IAR has improved orbital accuracy in all three directions. The reduction of the once-per-revolution systematic effects in the along-track direction is to be noticed, in particular, with an improvement in the along-track orbital accuracy of over 50% when using the COM final products. Compared with the reference orbits provided by the Copernicus POD service, the 3D RMS of the IAR-enabled orbital errors are about 1 to 1.5 cm in all single- and dual-constellation scenarios when using the COM final products. When using the GFZ rapid products, the 3D RMSE is about 2 cm in the single-constellation scenarios and amounts to about 1.4 cm in the GPS+Galileo combined scenario.

ACKNOWLEDGMENTS

This work is funded by the National Time Service Center, Chinese Academy of Sciences (CAS) (No. E167SC14), the National Natural Science Foundation of China (No. 12203059), the CAS "Light of West China" Program (XAB2021YN25), the Australian Research Council—discovery project (No. DP 190102444), and the Shaanxi Province Key R&D Program Project (2022KW-29). We also acknowledge the support of the international GNSS monitoring and assessment system (iGMAS) at the National Time Service Center, and the National Space Science Data Center, National Science & Technology Infrastructure of China (http://www.nssdc.ac.cn).

REFERENCES

Allahvirdi-Zadeh, A., Wang, K., & El-Mowafy, A. (2021). POD of small LEO satellites based on precise real-time MADOCA and SBAS-aided PPP corrections. *GPS Solutions, 25*, 31. https://doi.org/10.1007/s10291-020-01078-8

Chen, L., Jiao, W., Huang, X., Geng, C., Ai, L., Lu, L., & Hu, Z. (2013). Study on signal-in-space errors calculation method and statistical characterization of BeiDou navigation satellite system. In Proceedings of the China Satellite Navigation Conference (CSNC) 2013; Sun J, Jiao W, Wu H, Shi C, Eds.; Lecture Notes in Electrical Engineering, Volume 243; Springer: Berlin, Heidelberg, Germany.

CSPDH (2023). Copernicus Sentinels POD Data Hub. Copernicus Open Access Hub, Europen Space Agency. Accessed on January 24, 2023 at https://scihub.copernicus.eu/gnss

Dach, R., Lutz, S., Walser, P., & Fridez, P. (2015). Bernese GNSS software version 5.2. User manual, Astronomical Institute, University of Bern, Bern Open Publishing. https://doi.org/10.7892/boris.72297

Deng, Z., Nischan, T., & Bradke, M. (2017). Multi-GNSS Rapid Orbit-, Clock- & EOP-Product Series. GFZ Data Services. https://doi.org/10.5880/GFZ.1.1.2017.002

Duan, B. & Hugentobler, U. (2021). Comparisons of CODE and CNES/CLS GPS satellite bias products and applications in Sentinel-3 satellite precise orbit determination. GPS Solutions, 25, 128. https://doi.org/10.1007/s10291-021-01164-5

Faragher, R., & Ziebart, M. (2020). OneWeb LEO PNT: Progress or Risky Gamble? *Inside GNSS*, September 28, 2020. https://insidegnss.com/oneweb-leo-pnt-progress-or-risky-gamble/

Folkner, W.M., Williams, J.G., & Boggs, D.H. (2009). JPL Interplanetary Network Progress Report 24-178, 2009

Ge, H., Li, B., Ge, M., Zang, N., Nie, L., Shen, Y., & Schuh, H. (2018). Initial assessment of precise point positioning with LEO enhanced global navigation satellite systems (LeGNSS). *Remote Sensing*, *10*(7), 984. https://doi.org/10.3390/rs10070984

Geng, J., Zhang, Q., Li, G., Liu, J., & Liu, D. (2022). Observable-specific phase biases of Wuhan multi-GNSS experiment analysis center's rapid satellite products. Satellite Navigation, 3, 23. https://doi.org/10.1186/s43020-022-00084-0

GPS World Staff (2017). PNT Roundup: Iridium constellation provides low-Earth orbit satnav service. GPS World, January 12, 2017. https://www.gpsworld.com/iridium-constellation-provides-low-earth-orbit-satnav-service/#:~:text=Based%20on%20the%20low%2DEarth,buildings%20and%20other%20difficult%20locations.

Hauschild, A,, Tegedor, J., Montenbruck, O., Visser, H., & Markgraf, M. (2016) Precise onboard orbit determination for LEO satellites with real-time orbit and clock corrections. *In Proc. ION GNSS+ 2016*, Institute of Navigation, Portland, Oregon, USA, September 12-16, 3715-3723.

Hauschild, A., Montenbruck, O., Steigenberger, P., Martini, I., & Fernandez-Hernandez, I. (2022). Orbit determination of Sentinel-6A using the Galileo high accuracy service test signal. *GPS Solutions*, *26*, 120. https://doi.org/10.1007/s10291-022-01312-5

Lawrence, D., Cobb, H. S., Gutt, G., O'Connor, M., Reid, T. G. R., Walter T., & Whelan, D. (2017). Innovation: Navigation from LEO. *GPS World*, June 30, 2017. https://www.gpsworld.com/innovation-navigation-from-leo/

Li, X., Ma, F., Li, X., Lv, H., Bian, L., Jiang, Z., & Zhang, X. (2018a). LEO constellation-augmented multi-GNSS for rapid PPP convergence. *Journal of Geodesy*, *93*, 749-764. https://doi.org/10.1007/s00190-018-1195-2

Lyard, F., Lefevre, F., Letellier, T., & Francis, O. (2006). Modelling the global ocean tides: Modern insights from FES2004. *Ocean Dyn.*, *56*, 394–415.

Männel, B., Brandt, A., Nischan, T., Brack, A., Sakic, P., & Bradke, M. (2020). GFZ rapid product series for the IGS. GFZ Data Services. https://doi.org/10.5880/GFZ.1.1.2020.003

Mao, X., Arnold, D., Girardin, V., Villiger, A., & Jäggi, A. (2021). Dynamic GPS-based LEO orbit determination with 1 cm precision using the Bernese GNSS Software. *Advances in Space Research, 67*(2): 788-805. https://doi.org/10.1016/j.asr.2020.10.012

Michalak, G., Glaser, S., Neumayer, K. H., König, R. (2021). Precise orbit and Earth parameter determination supported by LEO satellites, inter-satellite links and synchronized clocks of a future GNSS. *Advances in Space Research, 12*, 4753–4782. https://doi.org/10.1016/j.asr.2021.03.008

Montenbruck, O., & Gill, E. (2000). Around the world in a hundred minutes. *Satellite orbits, 1st ed.;* Springer: Berlin, Heidelberg, Germany, 1–13.

Montenbruck, O., Hauschild, A., Andres, Y., von Engeln, A., & Marquardt, C. (2013). (Near-) real-time orbit determination for GNSS radio occultation processing. *GPS Solutions*, *17*, 199-209. https://doi.org/10.1007/s10291-012-0271-y

Montenbruck, O., Hackel, S., Wermuth, M., & Zangerl, F. (2021). Sentinel-6A precise orbit determination using a combined GPS/Galileo receiver. *Journal of Geodesy, 95*(9), 109. https://doi.org/10.1007/s00190-021-01563-z

Pavlis, N.K., Holmes, S.A., Kenyon, S.C., & Factor, J.K. (2008). An Earth gravitational model to degree 2160: EGM2008. *EGU 2008*, Vienna, Austria, 13–18 April 2008.

Petit, G., & Luzum, B. (2010). IERS Conventions. IERS Technical Note, 36. Verlag des Bundesamtes für Kartographie und Geodäsie, Frankfurt am Main, Germany, 2010. 179p, ISBN 3-89888-989-6

Reid, T. G. R., Neish, A. M., Walter, T., & Enge, P. K. (2018). Broadband LEO constellations for navigation. *Navigation, Journal of the Institute of Navigation*, *65*(2), 205–220. https://doi.org/10.1002/navi.234

Reid, T., Banville, S., Chan, B., Gunning, K., Manning, B., Marathe, T., Neish, A., Perkins, A., & Sibois, A. (2022). PULSAR: A New Generation of Commercial Satellite Navigation. *ION GNSS+ 2022*, September 11-15, 2023, Denver, Colorado, USA

Schaer, S., Villiger, A., Arnold, D., Dach, R., Prange, L., & Jäggi, A. (2021). The CODE ambiguity-fixed clock and phase bias analysis products: Generation, properties, and performance. *Journal of Geodesy*, *95*(7), 1–25.

Su, K., Jin, S., & Jiao, G. (2022). GNSS carrier phase time-variant observable-specific signal bias (OSB) handling: an absolute bias perspective in multi-frequency PPP. *GPS Solutions*, *26*, 71. https://doi.org/10.1007/s10291-022-01255-x

Villiger, A., Schaer, S., Dach, R., Prange, L., Sušnik, A., & Jäggi, A. (2019). Determination of GNSS pseudo-absolute code biases and their long-term combination. *Journal of Geodesy*, *93*(9):1487–1500

Wang, K., Allahvirdi-Zadeh, A., El-Mowafy, A., & Gross, J. N. (2020). A Sensitivity Study of POD Using Dual-Frequency GPS for CubeSats Data Limitation and Resources. *Remote Sensing*, *12*(13), 2107. https://doi.org/10.3390/rs12132107

Wang, K., & El-Mowafy, A. (2020). Proposed orbital products for positioning using mega-constellation LEO satellites. *Sensors, 20*(20), 5806. https://doi.org/10.3390/s20205806

Wang, K., El-Mowafy, A., Wang, W., Yang, L., & Yang, X. (2022). Integrity Monitoring of PPP-RTK Positioning; Part II: LEO Augmentation. *Remote Sensing, 14*(7), 1599. https://doi.org/10.3390/rs14071599

Yang, L. (2019). The Centispace-1: A LEO Satellite-Based Augmentation System. *The 14th Meeting of the International Committee on Global Navigation Satellite Systems*, Bengaluru, India, 8 - 13 December 2019